

A LoRA is Worth a Thousand Pictures

Chenxi Liu¹ Towaki Takikawa² Alec Jacobson^{1,3}
¹University of Toronto ²Outerport ³Adobe Research

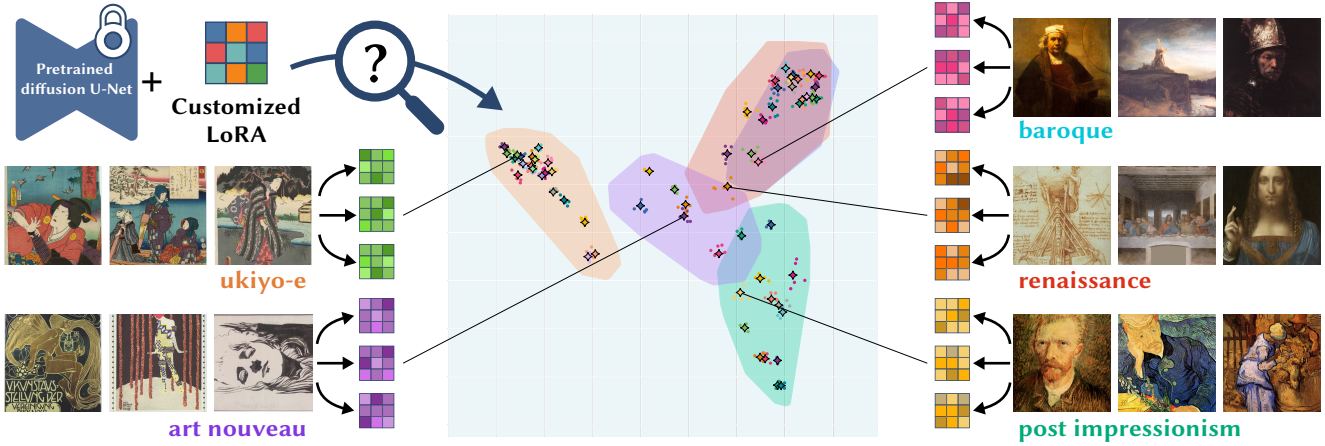


Figure 1. We show that LoRA weights trained on small artistic datasets can act as standalone feature representations by constructing an embedding of style-mimicking LoRAs trained on historic ArtBench artworks [36]. Genres are indicated by shaded convex hulls: **art nouveau**, **baroque**, **post impressionism**, **renaissance**, and **ukiyo-e**, with artists color-coded within each genre and centroids marked as stars. We show only 5 samples per artist to avoid visual clutter. See our supplementary materials for an interactive visualization.

Abstract

Recent advances in diffusion models and parameter-efficient fine-tuning (PEFT) have made text-to-image generation and customization widely accessible, with Low Rank Adaptation (LoRA) able to replicate an artist’s style or subject using minimal data and computation. In this paper, we examine the relationship between LoRA weights and artistic styles, demonstrating that LoRA weights alone can serve as an effective descriptor of style, without the need for additional image generation or knowledge of the original training set. Our findings show that LoRA weights yield better performance in clustering of artistic styles compared to traditional pre-trained features, such as CLIP and DINO, with strong structural similarities between LoRA-based and conventional image-based embeddings observed both qualitatively and quantitatively. We identify various retrieval scenarios for the growing collection of customized models and show that our approach enables more accurate retrieval in real-world settings where knowledge of the training images is unavailable and additional generation is required. We conclude with a discussion on potential future applications,

such as zero-shot LoRA fine-tuning and model attribution.

1. Introduction

Advances in diffusion models have catalyzed a new mode of creative expression, where technical artists can produce imagery through text, image controls, and more. Parameter-efficient fine-tuning (PEFT) has played a particularly important role in this development by enabling the low-cost customization of image generation models to follow a certain style or subject from a small number of images (10-20 or even fewer), with Low Rank Adaption (LoRA) [23] being a stand out method. The adoption of LoRA in creative communities have been remarkable, with model sharing platforms like Civit.ai hosting thousands of custom models contributed by its 4 million users. This proliferation of custom models creates a new need for efficient ways to analyze, compare, and retrieve artistic styles. We show that the LoRA weights themselves can be an effective descriptor of artistic styles, enabling rapid analysis and retrieval without requiring additional image generation, feature extraction, or knowledge about the training set (Fig. 2).

In recent previous work [4, 51, 53], style analysis has

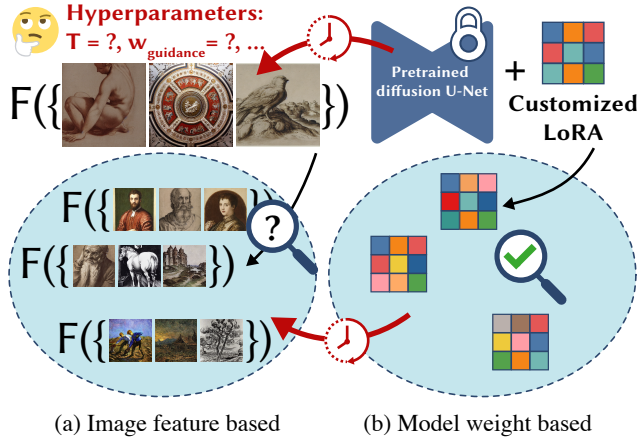


Figure 2. (a) Retrieving customized models based on image features requires additional image generation (red arrows), which depends on the choice of hyperparameters. (b) Direct retrieval of customized models using the model weights *themselves* is accurate and avoids extra costs as well as the need for choosing inference hyperparameters, including noise image seeds and prompts.

been approached through pre-trained vision models like CLIP [41] and DINO [6], which provide general-purpose embeddings capable of capturing style. Other works have also shown that model weights can be used for semantic image editing [9], 3D shape generation [11], and detect harmful language generation models [37]. However, the direct relationship between the LoRA weights and high-level image attributes (such as artistic style) for tasks like retrieval remains an open question.

In this work, we investigate whether LoRA weights trained on small artistic datasets can serve as standalone feature representations. Our findings include that while common pre-trained models produce clear style-distinguishable embeddings, LoRA weights provide even more well-separated embeddings. Furthermore, the artistic style embeddings derived from LoRA weights show a strong structural alignment, qualitatively and quantitatively, with those produced by these pre-trained models, suggesting a meaningful correspondence across different style embeddings.

By demonstrating that the embedding space of LoRA weights correspond to artistic style, our work enables new approaches for retrieving from and organizing the growing collection of custom models. This capability is particularly valuable for creative AI communities (e.g., Civitai¹), where it can help practitioners find similar styles, avoid duplicate fine-tuning, and detect unauthorized style mimicry. Furthermore, it can support new systems of attribution and compensation such that artists can be properly credited for their contribution to a dataset for fine-tuning [10].

¹A site for sharing, inferring, merging, and training text-to-image models, including LoRAs.

2. Related Work

We begin by reviewing the prior-arts of text-to-image generation, customization, and their connection to style. We then cover methods that attempt to computationally represent style. Finally, we discuss weight-space representations more generally, and motivate how LoRA weights can be suitable as an embedding space.

2.1. Text-to-image generation

Recent advances in text-to-image generation have revolutionized content creation workflows. Diffusion models [20, 21] are particularly effective at generating images from text descriptions, and Latent Diffusion models (LDMs) [42] enabled the generation of higher-resolution images by performing the denoising processes in a lower-resolution latent space of a variational autoencoder.

The release of Stable Diffusion, a pre-trained LDM trained on large-scale datasets, created a creative community around customizing these open source models via fine-tuning on specific artistic styles. Dreambooth [43] and MultiDiffusion [33] present a set of techniques to customize diffusion models through fine-tuning, while the open-source community adopt Low Rank Adaptation (LoRA) [23] for more efficient fine-tuning despite being originally proposed for Large Language Models. Several works augment the LoRA fine-tuning framework for different artistic applications. MuseumMaker [38] adopts a continual learning framework to mix an arbitrary number of artistic styles in a streaming manner. ZipLoRA [48] proposes an alternate method of mixing LoRA weights (beyond simple linear combination) that takes into account subject-style interference. B-LoRA [15] empirically finds LoRA weight components that correspond to style and subject for separate control. These works hint towards a connection between the weights of the LoRA and artistic style. In our work, we explore the extent to which the embedding space of the LoRA weights correspond to style.

2.2. Style Representation

The notion of style can be interpreted in several different ways, but we use the definition in art history: [style is] *a distinctive manner which permits the grouping of works into related categories*, posed by Eric Fernie [13, 39]. Humans excel at recognizing styles — by recognizing brushstroke patterns, color palette, and compositional preferences, humans can quickly distinguish between a painting by Van Gogh and Hokusai. To computationally emulate this capability, we frame style analysis as a clustering problem: we seek computational representations of images where artworks naturally group together in ways that mirror how humans categorize art by style.

Early methods extract low-level image statistics such as Fractal analysis [52], brush stroke wavelets [27], sparse

coding [24], and color statistics [31] to quantify artistic styles. Deep learning gave rise to methods [29] that use pre-trained neural networks to embed images, with applications like style-transfer [16, 28], perceptual image differencing [28, 57], and style analysis [44, 45]. Later works use transformers [6, 8] to achieve improved performance for classification. Notably, CLIP [41] trains a model which embeds images and corresponding textual labels into a shared embedding space, giving the space more semantic structure. CLIP is found to be a particularly effective embedding space for artistic works, with several works [4, 51, 53] measuring the efficacy of CLIP and fine-tuned CLIP or DINO embeddings for artistic style analysis.

In contrast to works that use a feature extraction mechanism such as low-level image statistics or the feed-forward pass of an embedding network to analyze style, our work uses *fine-tuning* as a method of embedding a collection of images into a LoRA weight vector. This is particularly effective for our purposes of analyzing the collection of fine-tuned LoRA models available on the internet, as no additional inference (which introduces stochasticity and prompt engineering) is required to analyze a model. We additionally find that the embedding space of the LoRA weights better correspond to artistic style in comparison.

2.3. Weight Space Representations

The weights of a neural network are used as an embedding space in various settings. For example, HyperNetworks [18] use a neural network to predict the weights of another neural network, and has been adopted for applications like image editing [3] and 3D shape generation [11]. As another example, neural fields [56] emerged as a paradigm where neural networks fit to specific objects and scenes were treated as first-class data types [7]. Weights2weights [9] explores LoRA weights as an embedding space for semantic editing of images, similar to editing in a StyleGAN [30] embedding space. Lim et al [37] use LoRA weights as an input of another neural network that predicts the performance of the fine-tuned model. Similarly to these works, we treat LoRA weights as an embedding space for style analysis.

A core assumption in treating the fine-tuned weights as an embedding is that the space of fine-tuned models is smoothly structured and semantically meaningful. Several works explore properties in which this assumption can hold for neural networks. Frankle et al [14] show that when two models share the first k training iterations (where k is relatively small), they become *linearly mode connected*, meaning that linear interpolations between fine-tuned models share similar training, test loss, and similar performance. Zhou et al [59] demonstrate that linear mode connectivity can extend to intermediate feature maps and not just model weights. Linear mode connectivity has inspired weight-space ensemble methods, such as interpolating weights to

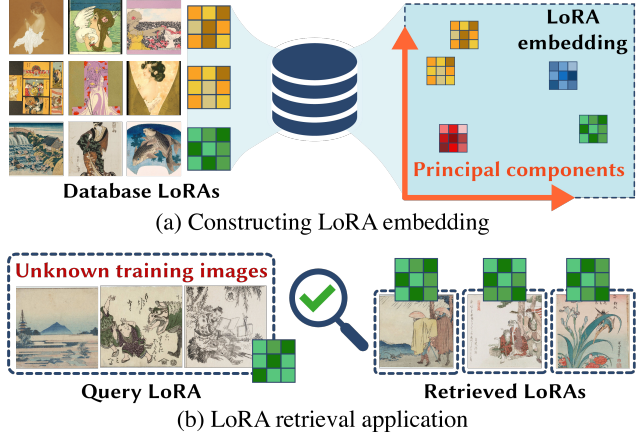


Figure 3. (a) We construct an embedding of style-customized LoRAs via PCA. (b) This embedding enables applications such as retrieval using a query LoRA trained on unknown images, avoiding the need for additional image generation.

reduce overfitting [55] or modify task-specific capabilities [25]. These concepts extend to LoRA weights, which all start from a pre-trained model which satisfies the condition for linear mode connectivity.

3. Method

We introduce a method to construct style embeddings *directly* from Low-Rank Adaptation (LoRA) weights instead of embedding the inferred images. We use PCA to project LoRA to a lower-dimensional space (Sec. 3.2) and introduce a calibration to improve the projection accuracy on unseen LoRAs (Sec. 3.3).

3.1. Low-Rank Adaptation (LoRA)

Our method constructs style embeddings from LoRA weights. LoRA is a technique used to fine-tune pre-trained base models to a downstream task based on a task-specific training set. The fine-tuning involves updating the pre-trained linear weight matrices $\mathbf{W}_0 \in \mathbb{R}^{m \times n}$ with update matrices $\Delta \mathbf{W}$ such that the forward pass is:

$$h = (\mathbf{W}_0 + \Delta \mathbf{W})x \quad (1)$$

This update is applied to all linear weight matrices across the network. For simplicity, we illustrate using a single matrix as an example.

Observing that $\Delta \mathbf{W}$ typically has a low intrinsic rank, LoRA reparameterizes this update matrix as $\Delta \mathbf{W} = \mathbf{B}\mathbf{A}$, where $\mathbf{B} \in \mathbb{R}^{m \times r}$, $\mathbf{A} \in \mathbb{R}^{r \times n}$, and $r \ll \min(m, n)$ is a small rank chosen by the user. The forward pass becomes:

$$h = \mathbf{W}_0x + \mathbf{B}\mathbf{A}x. \quad (2)$$

By updating only \mathbf{B} and \mathbf{A} during fine-tuning, LoRA significantly reduces the number of parameters, resulting in lower

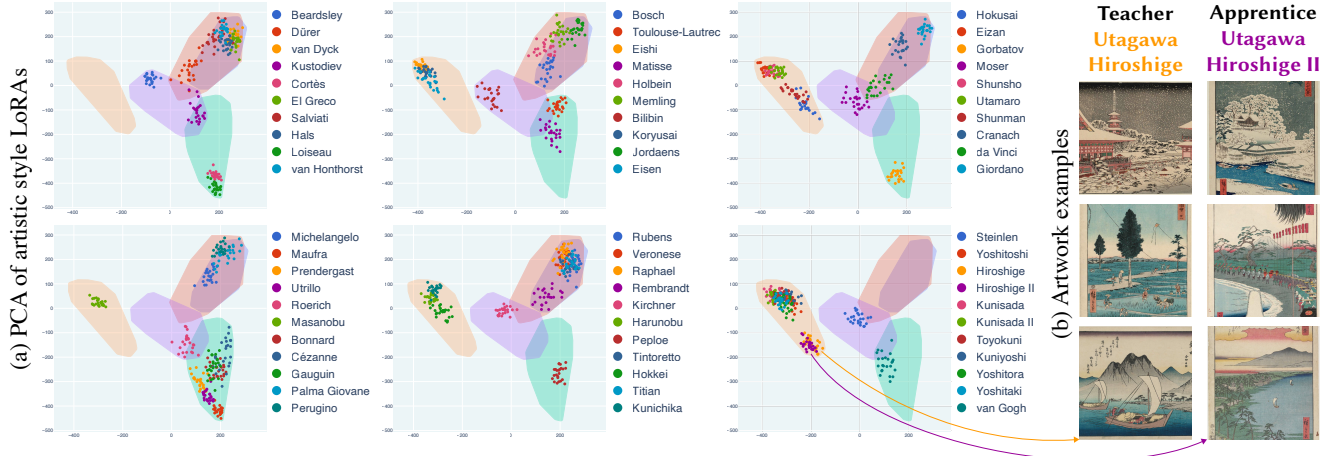


Figure 4. (a) Visualization of our artistic style LoRA embedding under the first two PCs. We use the same genre convex hulls as Fig. 1 and plot artist subsets across subfigures to avoid crowded visuals. (b) Samples are embedded in alignment with art historical knowledge; for example, a teacher and apprentice pair, known for sharing a similar style, are close in the embedding space.

training and storage costs.

We then flatten the new matrix components of the LoRA and concatenate them to obtain the LoRA vector θ :

$$\begin{aligned} \text{vec}(\mathbf{A}) &= [a_{11}, a_{12}, \dots, a_{rn}]^T \in \mathbb{R}^{rn \times 1} \\ \text{vec}(\mathbf{B}) &= [b_{11}, b_{12}, \dots, b_{mr}]^T \in \mathbb{R}^{mr \times 1} \\ \theta &= [\text{vec}(\mathbf{A}); \text{vec}(\mathbf{B})] \in \mathbb{R}^{(rn+mr) \times 1} \end{aligned}$$

The final θ concatenates all \mathbf{B} , \mathbf{A} across the entire network.

We use the LoRA weights trained on sets of images each created by a single artist to construct a database of LoRA weight vectors. As supported by linear mode connectivity and demonstrated by weight embedding and weight ensemble (Sec. 2.3), this LoRA embedding is smoothly structured and semantically meaningful.

3.2. Constructing Style Embeddings

We construct style embeddings from a collection of artists and their body of work, by sampling images from each artist’s body of work, fine-tuning a LoRA weight, and applying PCA to obtain a lower-dimensional style embedding which we will use for analysis.

Concretely, we build our style embedding based on ArtBench [36], a dataset of public domain historical artworks with authorship, genre, and other metadata (see Fig. 1, 3 for examples). For an artist i among the $n = 63$ artists with a sufficient number of artworks, we randomly sample 10 images from the training set to fine-tune a LoRA, yielding an unraveled weight vector $\theta_{i,j} \in \mathbb{R}^d$, where $d = 5,984,256$ in our setting (Fig. 3a; see Sec. 4.1 for experiment details).

Definitions We refer to LoRA models used to construct our database embeddings as *training LoRAs* and LoRAs that

are projected into this space (to query from the database) as *test LoRAs*. To test for robustness on different training setup (because test LoRAs may be arbitrary models from the community), we test on LoRAs that are trained with the same setup as the training LoRAs (defined as $\text{Test}[\text{Same}]$) as well as LoRAs that are trained with a different setup from the training set (defined as $\text{Test}[\text{Diff}]$). See Sec. 4.4 for our specific evaluation setup.

Fine-tuning To isolate the effect of LoRA weights from the text encoder, we fine-tune only the U-Net, without token optimization. Each LoRA is trained with a unique random identifier token $[V]$, inserted before an auto-caption for each image, with no textual hints associated with the specific artist. We verify that these automatic captions are free of information associated with the certain artist. We repeat this process to collect a dataset $\mathcal{D} = \{\theta_{i,j}\}$ with $m_{\text{train}} = 30$ LoRAs per artist.

Dimensionality reduction To obtain lower-dimensional embeddings, we apply PCA to \mathcal{D} and obtain the principal components (PCs) $\{\mathbf{q}_1, \dots, \mathbf{q}_k\}$, resulting in Fig. 4. We find that the weight vectors of LoRAs trained on images by the *same* artist cluster together closely, despite their training sets overlapping by only 39% on average and 50% at most, while LoRAs trained on images by *different* artists tend to be well-separated (quantitative evaluations in Sec. 4.3).

We observe that the subspace of the first two principal components aligns with art history prior knowledge (Fig. 4). For instance, the eastern genre (*ukiyo-e*) is distinctly separated from the western genres. Among the western genres, *art nouveau* is closest to *ukiyo-e*, reflecting the historical influence of *ukiyo-e* on *art nouveau* during its devel-

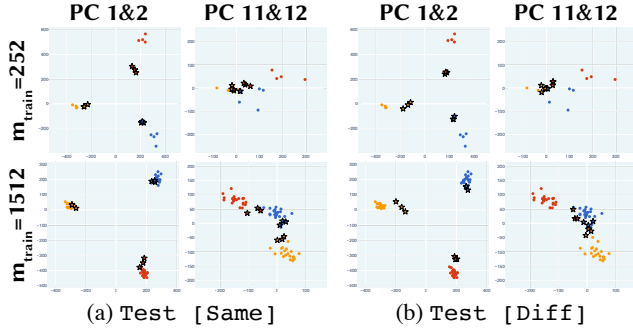


Figure 5. Visualization of the PCA plot of the training LoRAs (circles) and test LoRAs (stars). We see that with a smaller training set size (252 samples, top row), the embedding for the training and test LoRAs drift apart. Using a larger training set size (1512, bottom row) improves the drift, but the drift is still apparent for test LoRAs trained under different settings from the training LoRAs (Test [Diff], bottom right).

opment, as well as the shared medium of printmaking between the two. The overlapping artistic style clusters reflect known teacher-apprentice or influence relationships: [Utawaga Hiroshige](#), [Utawaga Hiroshige II](#), [Peter Paul Rubens](#), [Anthony van Dyck](#), and [Pietro Perugino](#), [Raphael](#). Several close artistic style clusters (e.g., [da Vinci](#), [Dürer](#), [Michelangelo](#)) also match prior quantitative analysis of artworks [5].

3.3. Calibrating for PCA Projection Errors

Using the PCA naively is suboptimal, as the PCA constructed from the train LoRAs is not robust enough to accurately generalize to the test LoRAs. We present a method to correct for the distribution difference.

Let \mathbf{Q} be the projection matrix with rows $\mathbf{q}_1, \dots, \mathbf{q}_k$. We observe that the straightforward projection $\pi(\boldsymbol{\theta}) = \mathbf{Q} \cdot \boldsymbol{\theta}$ introduces errors. The projection errors are caused by the limited amount of data with respect to the high dimensionality of data ($d = 5, 984, 256$), especially for the later PCs, which are more challenging to estimate accurately (see Fig. 5 for a visualization of the drift between the training and test LoRA embeddings). We introduce a simple calibration strategy to improve the generalization ability while avoiding the expensive generation of large-scale LoRA datasets.

Let $\boldsymbol{\theta}'_i$ be a LoRA weight vector of an artist i in the test LoRA set that is unseen by the PCA computation, and let $\{\boldsymbol{\theta}_{i,j} \mid i = 1, \dots, n, j = 1, \dots, m_{\text{train}}\}$ be the data that is fed to PCA. We find that in the embedding space (see stars in Fig. 5), test LoRAs stay clustered together (within artist labels), despite drifting away from corresponding training LoRA clusters. This implies a simple transformation can correct the drift with respect to the training LoRA clusters. We can calibrate the projection of a test LoRA weight vector using a small calibration set and doing a very simple variation of domain adaptation [12, 19, 40] for PCA by adapting

the training set PCA to the calibration set:

1. Split the training set into a PCA training set of m_{train} LoRAs and a small calibration set of m_{cali} LoRAs per artist ($m_{\text{cali}} = 3$ for all our experiments). Note that this calibration set is based on data available during training and is entirely disjoint from our validation and test data.
2. Compute the average LoRA weights per artist: $\bar{\boldsymbol{\theta}}'_i = \sum_j \boldsymbol{\theta}'_{i,j} / m_{\text{cali}}$, $\bar{\boldsymbol{\theta}}_i = \sum_j \boldsymbol{\theta}_{i,j} / m_{\text{train}}$.
3. Solve for $\mathbf{s} = \{s_1, \dots, s_k\}$ and $\mathbf{t} = \{t_1, \dots, t_k\}$

$$\begin{aligned} \min_{s_k, t_k} \frac{1}{2} \sum_i \|s_k \cdot \pi_k(\bar{\boldsymbol{\theta}}'_i) + t_k - \pi_k(\bar{\boldsymbol{\theta}}_i)\|^2, \\ S_k^1 = \sum_i \pi_k(\bar{\boldsymbol{\theta}}_i) \cdot \pi_k(\bar{\boldsymbol{\theta}}'_i), S_k^2 = \sum_i \pi_k(\bar{\boldsymbol{\theta}}'_i)^2, \\ S_k^3 = \sum_i \pi_k(\bar{\boldsymbol{\theta}}_i), S_k^4 = \sum_i \pi_k(\bar{\boldsymbol{\theta}}_i) \\ s_k = \frac{S_k^1 - (S_k^3 \cdot S_k^4) / n}{S_k^2 - (S_k^4)^2 / n}, t_k = \frac{S_k^3 - s_k \cdot S_k^4}{n}, \end{aligned} \quad (3)$$

We precompute \mathbf{s} , \mathbf{t} and define a new projection $\pi(\boldsymbol{\theta}', \mathbf{s}, \mathbf{t}) = \text{diag}(\mathbf{s}) \mathbf{Q} \cdot \boldsymbol{\theta}' + \mathbf{t}$ for unseen input LoRAs.

The construction of training and calibration sets (Step 1) varies according to the application and is described in Sec. 4.1. Furthermore, we observe that $t_k \approx 0$ when projecting Test [Same] LoRAs (Sec. 4.5), allowing a simplified calibration including only $s_k = S_k^1 / S_k^2$ (Step 3).

4. Experiments

4.1. Implementation Details

LoRA fine-tuning We utilize Stable Diffusion 1.5 [1, 42] as our pre-trained base model. We conduct LoRA fine-tuning using a popular online repository [47]. The fine-tuning objective contains the denoising term and DreamBooth fine-tuning term [43]. We restrict fine-tuning to U-Net, including all linear weights in self-attentions, cross-attentions, and feedforward neural networks. Our default setting uses rank $r = 16$, $\alpha = 8$, and 1760 fine-tuning steps with learning rate 5×10^{-4} and Adam optimizer [32].

Dataset Since Stable Diffusion 1.5 is trained on 512×512 images, we select sufficiently large ArtBench original images, resize, and center crop to 512×512 . We pick artists with sufficient number of artworks (≥ 100), resulting in $n = 63$ artists from five genres (art nouveau, baroque, post impressionism, renaissance, ukiyo-e). For each artist, we reserve 15 images for validation and test respectively. For each preprocessed image, we automatically generate captions with the LAVIS [34] implementation of BLIP [35].

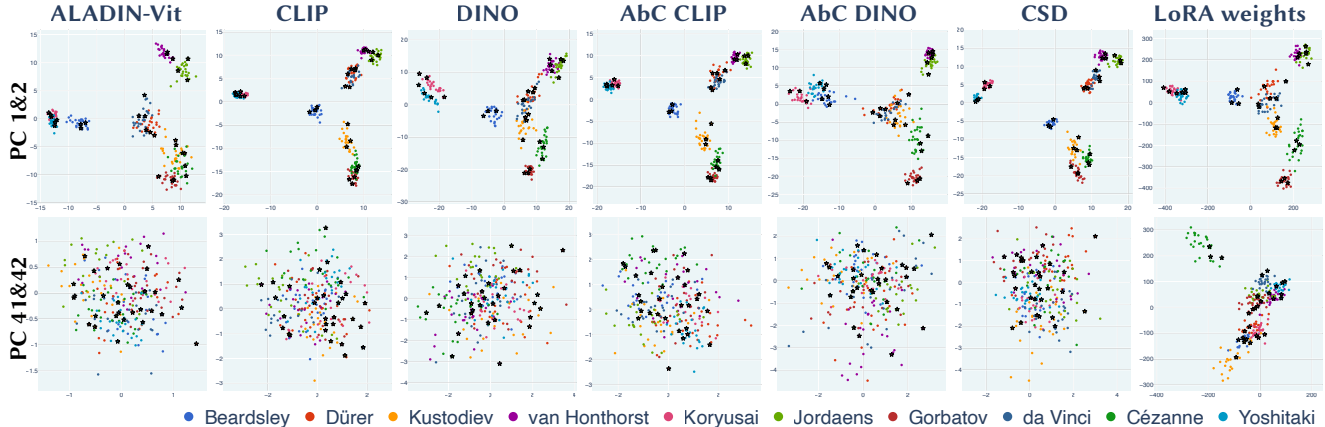


Figure 6. PCA visualizations of image features and LoRA weights (ours). The embeddings from different approaches are similar along the first few PCs, but only the LoRA weights maintain distinct style clusters in the later axes while others become more entangled. The PCA computations are performed on the entire training set. For clarity, we select only 10 artists for visualization.

Table 1. Quantitative clustering metrics. The training samples consist of data used to construct the embeddings. The test samples are data not seen during the embedding construction. Higher is better for both metrics.

Methods	ARI \uparrow (%)		NMI \uparrow (%)	
	Training	Test	Training	Test
ALADIN-ViT	79.2 \pm 3.0	77.5 \pm 3.5	93.9 \pm 0.8	96.5 \pm 0.5
CLIP	84.8 \pm 4.2	82.2 \pm 5.3	96.0 \pm 1.0	97.3 \pm 0.9
DINO	75.9 \pm 3.3	73.2 \pm 3.5	92.7 \pm 0.9	95.3 \pm 0.6
AbC CLIP	79.1 \pm 3.3	74.4 \pm 4.2	94.5 \pm 0.7	95.9 \pm 0.6
AbC DINO	85.1 \pm 2.6	84.7 \pm 3.7	96.0 \pm 0.7	97.8 \pm 0.6
CSD	84.1 \pm 3.0	82.0 \pm 3.7	96.0 \pm 0.7	97.5 \pm 0.6
Ours w/o cali	-	16.7 \pm 8.9	-	82.0 \pm 4.5
Ours	96.0\pm2.1	95.6\pm2.5	99.2\pm0.4	99.5\pm0.3

Data split For our clustering experiment, we split our training LoRA set (24 per artist) into an actual training set ($m_{\text{train}} = 21$) and a calibration set ($m_{\text{cali}} = 3$). For our retrieval experiment, we use a training set with $m_{\text{train}} = 24$ and create a calibration set ($m_{\text{cali}} = 3$) generated based on the training image set.

4.2. Comparison Settings

We compare against common image features, including style descriptor (ALADIN-ViT [45]), self-supervised (DINO [6]), language pre-trained (CLIP [41]) and image attribution fine-tune (AbC CLIP, AbC DINO with artist-style mapping [53], CSD [51]). Let $F(\cdot)$ be an image encoding function. Since a LoRA is trained on a small set of images $\{\mathbf{x}_1, \dots, \mathbf{x}_m\}$, for fair comparison, we compute a single image-feature sample through *aggregation*: $F(\{\mathbf{x}_1, \dots, \mathbf{x}_m\}) = \sum_{j=1, \dots, m} F(\mathbf{x}_j)/m$.

4.3. Clustering

We first evaluate the clustering performance of different embedding methods to see how well the clusters correspond to artistic styles. We apply k-means with $k = 63$ to embeddings of the training samples, either directly as comparison image features or through PCA computation in our method. Then, we cluster and report three types of input samples: training samples (24 per artist), validation samples (3 per artist) and test samples (3 per artist). We measure common clustering metrics: Adjusted Rand Index (ARI) and Normalized Mutual Information (NMI). Each reported number is averaged over 10 results with different random seeds.

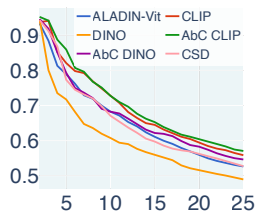
Visual comparison of PCA embeddings While we quantitatively evaluate the comparison methods directly using their high-dimensional features, PCA visualizations in Fig. 6 provide an opportunity for visual evaluations and insightful observations. Qualitatively, the embeddings (whether represented by LoRA weights or aggregated image features) of subsets of artworks by the same artists should be closer to each other than to those from other artists. We observe that the embeddings from various approaches show similarities along the first two PCs. However, as we examine the later PCs, the LoRA weights embedding continues to produce well-separated style clusters up to approximately the 42nd axis, while the comparisons become more entangled.

Quantitative clustering performance We report ARIs and NMIs in Table 1. Our approach generalizes well after calibration, achieving similar performance on both the training and test sets and outperforming all comparisons. These differences may be attributed to the greater amount

of information captured by the LoRA weights, as visualized and discussed above.

Embedding similarity

We quantify the similarity between PCA embeddings by measuring the cosine similarity (\uparrow , $[-1, 1]$) between corresponding samples with increasing PCA dimensions (inset). The results show that embeddings with the first two PCs exhibit high similarity ($[0.93, 0.95]$), but this similarity diminishes as additional PCs are included. To ensure a meaningful comparison, we vary PC signs to optimally align the two embeddings.



4.4. Retrieval

We then evaluate how well the embeddings can be used for a style-based retrieval task. Given a query LoRA trained on images by a single artist from our benchmark dataset, we retrieve the top matches using k-nearest neighbors ($k = 24$, the total number of instances per artist in our setting), using cosine distance for all baselines and Euclidean distance for our method. We test query LoRAs trained on image sets of size 3, keeping other training configurations consistent. These image sets only include images from our reserved validation or test sets (15 images per artist respectively), ensuring *no overlap* with the embedding training sets. We measure two standard recommendation system metrics: mean Average Precision (mAP) and Recall@k. Each number reported is averaged over 5 queries per artist, resulting in a total of 315 queries.

We perform comparisons against aggregated image features under two different scenarios in which LoRA weights are shared in the community. (1) *Original*: the LoRA weights are shared alongside the LoRA’s training set, allowing features to be computed from the original artwork images. (2) *Generated*: the LoRAs weights are shared on their own, requiring prompts to generate sample images for feature computation, incurring additional costs (Fig. 2). For a fair comparison, we reduce the challenges for the comparison approaches by generating sample images using automatic captions of the original training images as prompts. We observe that LoRAs, particularly those trained on small image sets, tend to memorize the original training images with only minor variations in detail, creating a more favorable condition for the comparison approaches to perform effectively. As far as we know, in current online communities, LoRAs are rarely shared with their training images, making the *generated* scenario more realistic. These two scenarios can affect query and embedding respectively, resulting in four comparison settings.

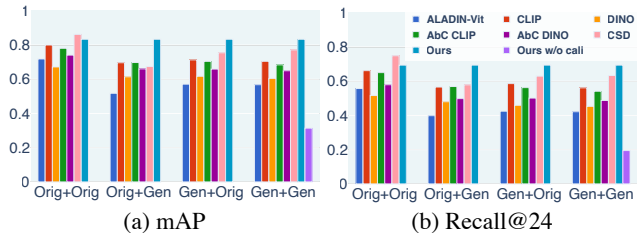


Figure 7. Retrieval metrics. Our approach uses the same strategy across all four retrieval scenarios ($[\text{Embedding}] + [\text{Query}]$) and produces the same metrics. *Orig* refers to the setting where the original training set is available, and *Gen* refers to the setting where only generated images (from the LoRA) are available.

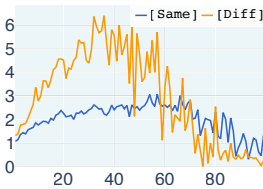
Using original training images The setting of using original images for both query and embedding essentially applies our approach as an image feature extractor. As shown in Fig. 7 under the *Orig+Orig* setting, our approach outperforms all comparisons, including common features such as CLIP and DINO, with the exception of the recent CSD feature. Although applying our approach for image feature extraction is impractical due to the additional LoRA training required, this stress test demonstrates that our method is robust even under challenging conditions, such as when dataset LoRAs and query LoRAs share no training images.

Using generated images Among the three settings involving generated images (Fig. 7), *Gen+Orig* represents the retrieval of LoRAs using actual artist-created images; *Gen+Gen* refers to the retrieval of LoRAs using a LoRA model with an unknown training set; and *Orig+Gen* is less realistic as it requires constructing an entire dataset embedding based on the original training images. Our approach achieves significantly better performance in both mAP and Recall@24 without requiring additional inferences.

4.5. Ablations

PCA We compute 100 PCs based on our database LoRAs and use the same PCA result for both tasks, with different number of PCs: 67 for clustering, 69 for retrieval. These numbers are determined through grid search using our validation set. See our supplemental for detailed results.

Calibration We verify using our validation set that our calibration produces better-aligned projections in both types of test LoRAs (Fig. 8). The performance improvements on test sets for clustering and retrieval are presented in Table 1 and Fig. 7 respectively (“Ours w/o cali” vs. “Ours”). Empirically, we observe that $s_1 \approx 1$; $s_{k_1} < s_{k_2}$ when



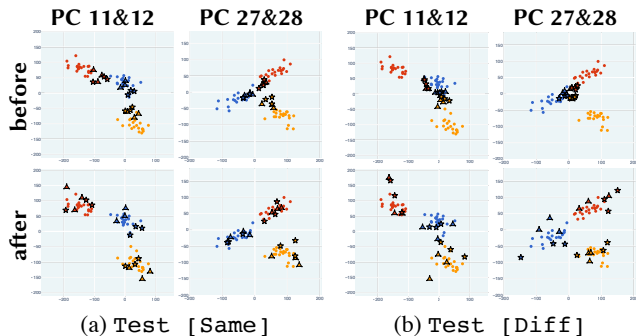


Figure 8. Our calibration method corrects for the drift between the training LoRA embeddings (circle) and the test LoRA embeddings (triangle) by using the hold-out calibration set (star) to calibrate. Before the calibration, the test LoRA embeddings are misaligned from the train LoRAs (top row). After calibration, the distributions are closer together (bottom row). Our method generalizes reasonably to test LoRAs that are trained under a different configuration from the training LoRAs (bottom right).

$k_1 < k_2$ until approximately PC 70 and 40 for projecting `Test [Same]` and `Test [Diff]` LoRAs respectively, when the projections become too inaccurate for effective calibration (inset). To ablate our choice of only solving for s when projecting unseen database LoRAs, we report $t_k < 4.5 \times 10^{-3} \approx 0$ under min-max normalization per PC.

Sub-networks Applying LoRA to a subset of the network, often cross-attention layers, is a common practice for efficient fine-tuning, adopted by both practitioners [46] and in research [9, 15, 33, 48]. Given our models with LoRA applied to the entire U-Net, we investigate the style representation capabilities of different components under our training configuration. For fair comparison, we evaluate clustering performance based on our training set, using the optimal number of principal components (PCs). Let d be the dimension of the full-network LoRA vectors. The ARIs are: full network (96.0%, d), feedforward neural networks (97.5%, $0.47d$), self-attention (94.4%, $0.27d$), and cross-attention (85.6%, $0.27d$). These results suggest that, despite the common practice, when applying LoRA to the full U-Net, cross-attention layers are less representative of style compared to self-attention and feedforward neural networks. Notably, the feedforward network demonstrates slightly better representation capability than the full network. Further investigations into models with LoRA applied only to sub-networks present an interesting future direction. See our supplemental for detailed results.

5. Discussions and Future Directions

We have demonstrated that LoRA weights trained on small artistic datasets can function as standalone feature represen-

tations. We achieve more accurate style-based clustering than image-based features. We show that retrieval is now possible with LoRA-query and LoRA-databases directly, outperforming image-based retrieval when training images are not and matching performance otherwise.

Limitations All the LoRAs we examined are trained with the same number of training steps, requiring roughly 5-10 minutes on our mid-tier and high-end GPUs. It would be interesting to generalize our results to LoRAs with fewer training steps (improving speed) or varied steps (improving generality). While disabling text encoder fine-tuning allows us to isolate our findings, text encoders are important in practice and their effect on LoRAs as artistic style representations should be investigated in the future. In each of our experiments, all LoRAs share the same dimensionality (e.g., rank or sub-network selection), but a potential untapped advantage of our method is that the PCA dimensionality could normalize heterogeneous LoRAs (see, e.g., [12]). LoRAs in the wild may be fine-tuned from different pre-trained checkpoints. While this breaks the linear mode connectivity assumptions, Ainsworth et al. [2] show that this can be resolved after finding certain permutations.

Future applications We hope to show how our work enables zero-shot LoRA fine-tuning: e.g., determining how to combine LoRAs from a database given some training images (generalizing our `Orig+Orig` setting). A concurrent work [26] proposes determining LoRA merging weights based on features computed on their corresponding training images. Our results show that image-feature spaces and LoRA weight spaces are deeply related but not by a simple similarity transform (as their method assumes). Therefore, we believe zero-shot training can be improved by working directly in LoRA weight space. Similarly, we hope to move beyond data attribution [17, 54, 58] to model attribution directly with LoRA weights, following the trends in popular use, sharing, and merging of LoRAs.

We envision our work to be a step toward a mutually beneficial relationship between professional artists and generative technology. While not extending generative *capabilities*, our work offers an alternative lens to analyze images, genres, and styles. For example, this could support style quantification and comparison tools that help artists develop their personal styles. Our work immediately enables better retrieval for existing online LoRA communities. Unauthorized style mimicry within these communities is a major concern of professional artists that is not yet fully resolved [22] by data “cloaking” and poisoning [49, 50]. Better tools for style analysis and attribution could foster more trustworthy, open, and mutually beneficial text-to-image ecosystems.

References

- [1] Stable-Diffusion-v1-5 checkpoint. <https://huggingface.co/stable-diffusion-v1-5/stable-diffusion-v1-5>. Accessed: 2024-11-06. 5
- [2] Samuel K Ainsworth, Jonathan Hayase, and Siddhartha Srinivasa. Git re-basin: Merging models modulo permutation symmetries. *arXiv preprint arXiv:2209.04836*, 2022. 8
- [3] Yuval Alaluf, Omer Tov, Ron Mokady, Rinon Gal, and Amit Bermano. Hyperstyle: Stylegan inversion with hypernetworks for real image editing. In *Proceedings of the IEEE/CVF conference on computer vision and pattern recognition*, pages 18511–18521, 2022. 3
- [4] Kar Balan, Shruti Agarwal, Simon Jenni, Andy Parsons, Andrew Gilbert, and John Collomosse. Ekila: Synthetic media provenance and attribution for generative art. In *Proceedings of the IEEE/CVF Conference on Computer Vision and Pattern Recognition*, pages 913–922, 2023. 1, 3
- [5] Marco Bressan, Claudio Cifarelli, and Florent Perronnin. An analysis of the relationship between painters based on their work. In *2008 15th IEEE International Conference on Image Processing*, pages 113–116. IEEE, 2008. 5
- [6] Mathilde Caron, Hugo Touvron, Ishan Misra, Hervé Jégou, Julien Mairal, Piotr Bojanowski, and Armand Joulin. Emerging properties in self-supervised vision transformers. In *Proceedings of the IEEE/CVF international conference on computer vision*, pages 9650–9660, 2021. 2, 3, 6
- [7] Thomas Davies, Derek Nowrouzezahrai, and Alec Jacobson. On the effectiveness of weight-encoded neural implicit 3d shapes. *arXiv preprint arXiv:2009.09808*, 2020. 3
- [8] Alexey Dosovitskiy. An image is worth 16x16 words: Transformers for image recognition at scale. *arXiv preprint arXiv:2010.11929*, 2020. 3
- [9] Amil Dravid, Yossi Gandelsman, Kuan-Chieh Wang, Rameen Abdal, Gordon Wetzstein, Alexei A Efros, and Kfir Aberman. Interpreting the weight space of customized diffusion models. *arXiv preprint arXiv:2406.09413*, 2024. 2, 3, 8
- [10] Pablo Ducru, Jonathan Raiman, Ronaldo Lemos, Clay Garner, George He, Hanna Balcha, Gabriel Souto, Sergio Branco, and Celina Bottino. Ai royalties—an ip framework to compensate artists & ip holders for ai-generated content. *arXiv preprint arXiv:2406.11857*, 2024. 2
- [11] Ziya Erkoç, Fangchang Ma, Qi Shan, Matthias Nießner, and Angela Dai. Hyperdiffusion: Generating implicit neural fields with weight-space diffusion. In *Proceedings of the IEEE/CVF international conference on computer vision*, pages 14300–14310, 2023. 2, 3
- [12] Basura Fernando, Amaury Habrard, Marc Sebban, and Tinne Tuytelaars. Unsupervised visual domain adaptation using subspace alignment. In *Proceedings of the IEEE international conference on computer vision*, pages 2960–2967, 2013. 5, 8
- [13] Eric Fernie. *Art History and its Methods: A Critical Anthology*. Phaidon, London, 1995. 2
- [14] Jonathan Frankle, Gintare Karolina Dziugaite, Daniel Roy, and Michael Carbin. Linear mode connectivity and the lottery ticket hypothesis. In *International Conference on Machine Learning*, pages 3259–3269. PMLR, 2020. 3
- [15] Yarden Frenkel, Yael Vinker, Ariel Shamir, and Daniel Cohen-Or. Implicit style-content separation using b-lora. *arXiv preprint arXiv:2403.14572*, 2024. 2, 8
- [16] Leon A Gatys. A neural algorithm of artistic style. *arXiv preprint arXiv:1508.06576*, 2015. 3
- [17] Kristian Georgiev, Joshua Vendrow, Hadi Salman, Sung Min Park, and Aleksander Madry. The journey, not the destination: How data guides diffusion models. *arXiv preprint arXiv:2312.06205*, 2023. 8
- [18] David Ha, Andrew Dai, and Quoc V Le. Hypernetworks. *arXiv preprint arXiv:1609.09106*, 2016. 3
- [19] Sharon Hendy and Yehuda Dar. Tl-pca: Transfer learning of principal component analysis. *arXiv preprint arXiv:2410.10805*, 2024. 5
- [20] Jonathan Ho and Tim Salimans. Classifier-free diffusion guidance. *arXiv preprint arXiv:2207.12598*, 2022. 2
- [21] Jonathan Ho, Ajay Jain, and Pieter Abbeel. Denoising diffusion probabilistic models. *Advances in neural information processing systems*, 33:6840–6851, 2020. 2
- [22] Robert Hönig, Javier Rando, Nicholas Carlini, and Florian Tramèr. Adversarial perturbations cannot reliably protect artists from generative ai. *arXiv preprint arXiv:2406.12027*, 2024. 8
- [23] Edward J Hu, Yelong Shen, Phillip Wallis, Zeyuan Allen-Zhu, Yuanzhi Li, Shean Wang, Lu Wang, and Weizhu Chen. Lora: Low-rank adaptation of large language models. *arXiv preprint arXiv:2106.09685*, 2021. 1, 2
- [24] James M Hughes, Daniel J Graham, and Daniel N Rockmore. Quantification of artistic style through sparse coding analysis in the drawings of pieter bruegel the elder. *Proceedings of the National Academy of Sciences*, 107(4):1279–1283, 2010. 3
- [25] Gabriel Ilharco, Marco Tulio Ribeiro, Mitchell Wortsman, Suchin Gururangan, Ludwig Schmidt, Hannaneh Hajishirzi, and Ali Farhadi. Editing models with task arithmetic. *arXiv preprint arXiv:2212.04089*, 2022. 3
- [26] Pengfei Jin, Peng Shu, Sekeun Kim, Qing Xiao, Sifan Song, Cheng Chen, Tianming Liu, Xiang Li, and Quanzheng Li. Retrieval instead of fine-tuning: A retrieval-based parameter ensemble for zero-shot learning. *arXiv preprint arXiv:2410.09908*, 2024. 8
- [27] C Richard Johnson, Ella Hendriks, Igor J Bereznoy, Eugene Brevdo, Shannon M Hughes, Ingrid Daubechies, Jia Li, Eric Postma, and James Z Wang. Image processing for artist identification. *IEEE Signal Processing Magazine*, 25(4):37–48, 2008. 2
- [28] Justin Johnson, Alexandre Alahi, and Li Fei-Fei. Perceptual losses for real-time style transfer and super-resolution. In *Computer Vision—ECCV 2016: 14th European Conference, Amsterdam, The Netherlands, October 11–14, 2016, Proceedings, Part II 14*, pages 694–711. Springer, 2016. 3
- [29] Sergey Karayev, Matthew Trentacoste, Helen Han, Aseem Agarwala, Trevor Darrell, Aaron Hertzmann, and Holger Winnemoeller. Recognizing image style. *arXiv preprint arXiv:1311.3715*, 2013. 3

- [30] Tero Karras, Samuli Laine, Miika Aittala, Janne Hellsten, Jaakko Lehtinen, and Timo Aila. Analyzing and improving the image quality of stylegan. In *Proceedings of the IEEE/CVF conference on computer vision and pattern recognition*, pages 8110–8119, 2020. **3**
- [31] Daniel Kim, Seung-Woo Son, and Hawoong Jeong. Large-scale quantitative analysis of painting arts. *Scientific reports*, 4(1):7370, 2014. **3**
- [32] Diederik Kingma and Jimmy Ba. Adam: A method for stochastic optimization. In *International Conference on Learning Representations (ICLR)*, San Diego, CA, USA, 2015. **5**
- [33] Nupur Kumari, Bingliang Zhang, Richard Zhang, Eli Shechtman, and Jun-Yan Zhu. Multi-concept customization of text-to-image diffusion. In *Proceedings of the IEEE/CVF Conference on Computer Vision and Pattern Recognition*, pages 1931–1941, 2023. **2, 8**
- [34] Dongxu Li, Junnan Li, Hung Le, Guangsen Wang, Silvio Savarese, and Steven CH Hoi. Lavis: A library for language-vision intelligence. *arXiv preprint arXiv:2209.09019*, 2022. **5**
- [35] Junnan Li, Dongxu Li, Caiming Xiong, and Steven Hoi. Blip: Bootstrapping language-image pre-training for unified vision-language understanding and generation. In *ICML*, 2022. **5**
- [36] Peiyuan Liao, Xiuyu Li, Xihui Liu, and Kurt Keutzer. The artbench dataset: Benchmarking generative models with artworks. *arXiv preprint arXiv:2206.11404*, 2022. **1, 4**
- [37] Derek Lim, Yoav Gelberg, Stefanie Jegelka, Haggai Maron, et al. Learning on lorax: G_L-equivariant processing of low-rank weight spaces for large finetuned models. *arXiv preprint arXiv:2410.04207*, 2024. **2, 3**
- [38] Jinxu Lin, Linwei Tao, Minjing Dong, and Chang Xu. Diffusion attribution score: Evaluating training data influence in diffusion model. *arXiv preprint arXiv:2410.18639*, 2024. **2**
- [39] Hsueh-Ti Derek Liu. *Algorithms for Data-driven Geometric Stylization Acceleration*. PhD thesis, University of Toronto, 2023. **2**
- [40] Sinno Jialin Pan, James T Kwok, Qiang Yang, et al. Transfer learning via dimensionality reduction. In *AAAI*, pages 677–682, 2008. **5**
- [41] Alec Radford, Jong Wook Kim, Chris Hallacy, Aditya Ramesh, Gabriel Goh, Sandhini Agarwal, Girish Sastry, Amanda Askell, Pamela Mishkin, Jack Clark, et al. Learning transferable visual models from natural language supervision. In *International conference on machine learning*, pages 8748–8763. PMLR, 2021. **2, 3, 6**
- [42] Robin Rombach, Andreas Blattmann, Dominik Lorenz, Patrick Esser, and Björn Ommer. High-resolution image synthesis with latent diffusion models. In *Proceedings of the IEEE/CVF conference on computer vision and pattern recognition*, pages 10684–10695, 2022. **2, 5**
- [43] Nataniel Ruiz, Yuanzhen Li, Varun Jampani, Yael Pritch, Michael Rubinstein, and Kfir Aberman. Dreambooth: Fine tuning text-to-image diffusion models for subject-driven generation. In *Proceedings of the IEEE/CVF conference on computer vision and pattern recognition*, pages 22500–22510, 2023. **2, 5**
- [44] Dan Ruta, Saeid Motiian, Baldo Faieta, Zhe Lin, Hailin Jin, Alex Filipkowski, Andrew Gilbert, and John Collomosse. Aladin: All layer adaptive instance normalization for fine-grained style similarity. In *Proceedings of the IEEE/CVF International Conference on Computer Vision*, pages 11926–11935, 2021. **3**
- [45] Dan Ruta, Andrew Gilbert, Pranav Aggarwal, Naveen Marri, Ajinkya Kale, Jo Briggs, Chris Speed, Hailin Jin, Baldo Faieta, Alex Filipkowski, et al. Stylelabel: Artistic style tagging and captioning. In *European Conference on Computer Vision*, pages 219–236. Springer, 2022. **3, 6**
- [46] Simo Ryu. LoRA implementation. <https://github.com/cloneofsimo/lorax>. Accessed: 2024-11-06. **8**
- [47] Kohya S. sd-scripts repository. <https://github.com/kohya-ss/sd-scripts>. Accessed: 2024-11-06. **5**
- [48] Viraj Shah, Nataniel Ruiz, Forrester Cole, Erika Lu, Svetlana Lazebnik, Yuanzhen Li, and Varun Jampani. Ziplora: Any subject in any style by effectively merging lorax. 2023. **2, 8**
- [49] Shawn Shan, Jenna Cryan, Emily Wenger, Haitao Zheng, Rana Hanocka, and Ben Y Zhao. Glaze: Protecting artists from style mimicry by {Text-to-Image} models. In *32nd USENIX Security Symposium (USENIX Security 23)*, pages 2187–2204, 2023. **8**
- [50] Shawn Shan, Wenxin Ding, Josephine Passananti, Stanley Wu, Haitao Zheng, and Ben Y Zhao. Nightshade: Prompt-specific poisoning attacks on text-to-image generative models. In *2024 IEEE Symposium on Security and Privacy (SP)*, pages 212–212. IEEE Computer Society, 2024. **8**
- [51] Gowthami Somepalli, Anubhav Gupta, Kamal Gupta, Shramay Palta, Micah Goldblum, Jonas Geiping, Abhinav Shrivastava, and Tom Goldstein. Measuring style similarity in diffusion models. *arXiv preprint arXiv:2404.01292*, 2024. **1, 3, 6**
- [52] Richard P Taylor, Adam P Micolich, and David Jonas. Fractal analysis of pollock’s drip paintings. *Nature*, 399(6735): 422–422, 1999. **2**
- [53] Sheng-Yu Wang, Alexei A Efros, Jun-Yan Zhu, and Richard Zhang. Evaluating data attribution for text-to-image models. In *Proceedings of the IEEE/CVF International Conference on Computer Vision*, pages 7192–7203, 2023. **1, 3, 6**
- [54] Sheng-Yu Wang, Aaron Hertzmann, Alexei A Efros, Jun-Yan Zhu, and Richard Zhang. Data attribution for text-to-image models by unlearning synthesized images. In *NeurIPS*, 2024. **8**
- [55] Mitchell Wortsman, Gabriel Ilharco, Jong Wook Kim, Mike Li, Simon Kornblith, Rebecca Roelofs, Raphael Gontijo Lopes, Hannaneh Hajishirzi, Ali Farhadi, Hongseok Namkoong, et al. Robust fine-tuning of zero-shot models. In *Proceedings of the IEEE/CVF conference on computer vision and pattern recognition*, pages 7959–7971, 2022. **3**
- [56] Yiheng Xie, Towaki Takikawa, Shunsuke Saito, Or Litany, Shiqin Yan, Numair Khan, Federico Tombari, James Tompkin, Vincent Sitzmann, and Srinath Sridhar. Neural fields in visual computing and beyond. In *Computer Graphics Forum*, pages 641–676. Wiley Online Library, 2022. **3**
- [57] Richard Zhang, Phillip Isola, Alexei A Efros, Eli Shechtman, and Oliver Wang. The unreasonable effectiveness of

- deep features as a perceptual metric. In *Proceedings of the IEEE conference on computer vision and pattern recognition*, pages 586–595, 2018. 3
- [58] Xiaosen Zheng, Tianyu Pang, Chao Du, Jing Jiang, and Min Lin. Intriguing properties of data attribution on diffusion models. *arXiv preprint arXiv:2311.00500*, 2023. 8
- [59] Zhanpeng Zhou, Yongyi Yang, Xiaojiang Yang, Junchi Yan, and Wei Hu. Going beyond linear mode connectivity: The layerwise linear feature connectivity. *Advances in Neural Information Processing Systems*, 36:60853–60877, 2023. 3

A LoRA is Worth a Thousand Pictures

Supplementary Material

1. Example Prompts and Images

We fine-tune each LoRA with a unique random identifier token [V], images and automatically generated captions. Example training data is shown in Fig. 1.

We construct LoRAs under two settings, `Test [Same]` and `Test [Diff]`, using training image sets of different sizes, 10 and 3 respectively. As shown in Fig. 1, images generated using the auto-caption prompts of the training images exhibit reasonable visual quality, confirming the success of LoRA training. Moreover, the resulting LoRAs tend to memorize the training images, generating slightly altered versions, particularly when the training image set is as small as three (`Test [Diff]`). This behavior grants the comparison image-based features an advantage when computed on these generated images (corresponding to `Gen` in our retrieval evaluation). Notably, this favorable condition does not occur in real-world practice, where LoRAs are typically shared without any information about the training dataset, including the captions of the training images.

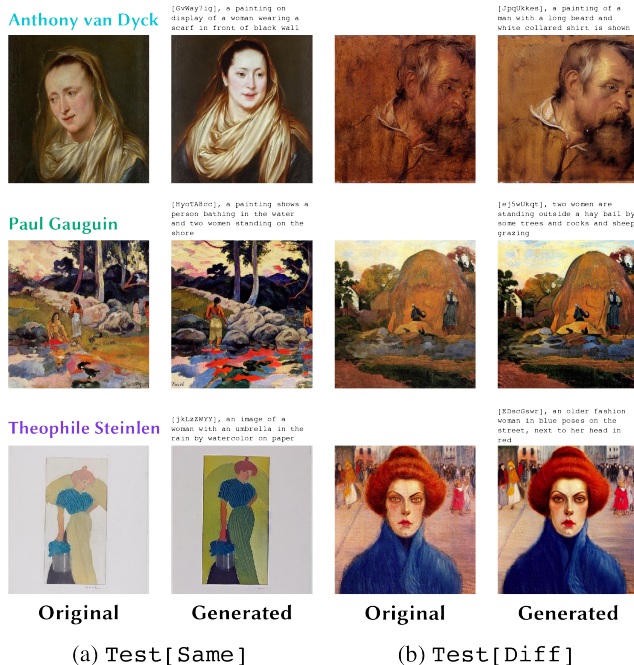


Figure 1. Example artworks used for LoRA training (“Original”) and images generated by the resulting LoRAs prompted by the automatic captions of the original images (“Generated”). These LoRAs tend to memorize the training images, especially when the training image set is small under the `Test [Diff]` setup.

2. Embedding Visualization

We provide interactive 2D and 3D visualization of our embedding. See `visualization_CVPR6545.html` in `interactive_visualization` folder. We provide a local HTML visualization instead of an external URL to comply with the updated CVPR policy.

3. Retrieval Results

We present in Fig. 2 the top 3 retrieval results for the comparisons and our method in the `Gen+Gen` setting (Sec. 4.4). While we show all three images used as query, due to the space limit, we only show one representative image out of ten for one database sample.

Despite these challenging queries, our approach consistently outperforms the comparisons, achieving near-perfect results. **Post impressionism** paintings, while uniquely stylized, share common visual characteristics such as vivid colors, thick application of paint, distinctive brushstrokes, and real-life subject matter like objects and outdoor scenes (Fig. 2a). Although most comparison methods retrieve results within the same genre and with similar content, most methods consistently fail to return correct results, with `AbC DINO` [53] and `CSD` [51] being only partially correct. Query 2 (Fig. 2b) is an interesting example consisting of Rembrandt’s sketches, a type of drawings not typically intended as finished works, which for Rembrandt were oil paintings. While our approach confuses the top 1 result with sketches by Dürer, all other methods perform worse, retrieving sketches by artists from a wide range of genres. The final example query demonstrates that our approach can distinguish subtle differences between teachers and apprentices (Fig. 2c). Similar to Query 1 (Fig. 2a), all comparison methods return `ukiyo-e` results, but the retrieved artists are incorrect. Interestingly, `CSD` selects Kunisada’s apprentice, Kunisada II, as its top 1 result, likely confused by the visual similarities between the teacher and apprentice.

4. Ablation Results

We provide detailed results for our ablation experiments: PCA and sub-networks (Sec. 4.5).

We visualize the performance curves of the full network on the validation set, showing ARI for clustering and mAP and Recall@24 for retrieval. As shown in Fig. 3, the performance increases sharply within the range [1, 15], peaks at the optimum, and then gradually declines.

We report in the main text the clustering performance (ARI) of three sub-networks: feedforward neural network



(a) Query 1

(b) Query 2

(c) Query 3

Figure 2. Example retrieval results. Artists' names are colored by the corresponding genres: **art nouveau**, **baroque**, **post impressionism**, **renaissance**, and **ukiyo-e**. Representative images of the retrieved results are framed in green for correct answers and red for incorrect ones.

Table 1. Retrieval performance comparison between image-based features and our approach using feedforward sub-network weights across different scenarios. Higher is better for both metrics.

Methods	mAP \uparrow (%)				Recall@24 \uparrow (%)			
	Orig+Orig	Orig+Gen	Gen+Orig	Gen+Gen	Orig+Orig	Orig+Gen	Gen+Orig	Gen+Gen
ALADIN-Vit	71.9	51.8	57.1	56.8	55.7	39.9	42.5	42.2
CLIP	80.0	69.7	71.3	70.5	66.2	56.6	58.6	56.2
DINO	67.2	61.4	61.7	60.5	51.6	48.0	45.9	45.3
AbC CLIP	78.1	69.8	70.5	68.4	65.0	56.9	56.3	54.1
AbC DINO	74.1	66.1	65.9	65.0	58.0	49.8	50.2	48.8
CSD	86.2	67.4	75.5	77.2	74.9	57.9	63.0	63.3
Ours w/o cali	31.8				19.5			
Ours	88.3				79.8			

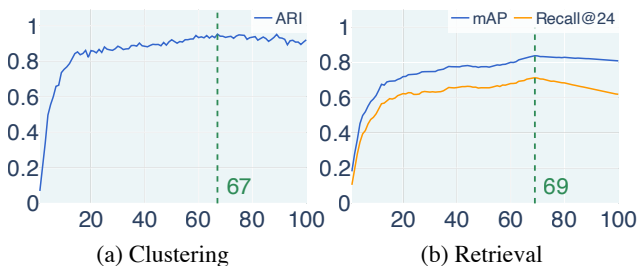


Figure 3. Clustering and retrieval performance as a function of the number of PCs. We determine the optimal number of PCs (indicated by green dashed lines) in Sec. 4.5 using the validation set.



Figure 4. Validation set clustering performances vary across different sub-networks: feedforward neural network (FF), self-attention (Self-Attn), and cross-attention (Cross-Attn).

(97.5%, 0.47d), self-attention (94.4%, 0.27d), and cross-attention (85.6%, 0.27d), where d is the dimension of the full network (96.0%, d). The ARI curves for these sub-networks on the validation set are shown in Fig. 4. While the feedforward network and self-attention exhibit similar behavior to the full network, the cross-attention sub-network, interestingly, has a different curve, with slower performance increases when the number of PCs is small.

We conduct an additional retrieval experiment using LoRA weights from the feedforward network, the sub-

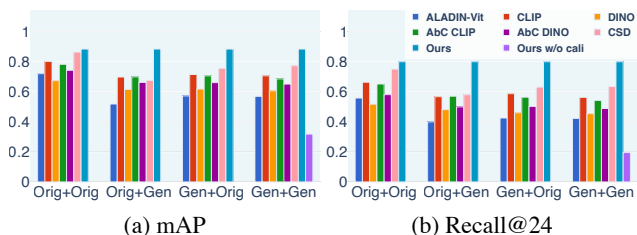


Figure 5. Our approach with feedforward sub-network weights outperforms all comparisons across all retrieval task scenarios.

network with the best performance evaluated in the clustering task. Through a grid search on the validation set, we determine the optimal number of PCs to be 62. This feedforward sub-network outperforms both the full network and all comparison methods even in the Orig+Orig setting (Fig. 5, Table 1). With approximately half the dimensionality of the full network and better clustering and retrieval performance, using feedforward sub-network weights to represent styles becomes a more effective choice. Notably, our experiments are conducted on LoRAs applied to the entire U-Net and whether this finding holds when only sub-network is fine-tuned remains an interesting question.

5. Detailed Statistics

We provide detailed metric statistics on training, validation, and test sets for our evaluation experiments, along with detailed measures for embedding similarity. The clustering performance (Table 1, Sec. 4.3) is fully presented in Table 2. The detailed measures for embedding similarity (inset in Sec. 4.3) are shown in Table 3. The retrieval metric statistics (Fig. 7, Sec. 4.4) are provided in Table 4.

Table 2. Quantitative clustering metrics. The training samples consist of data used to construct the embeddings. The test samples are data not seen during the embedding construction. Higher is better for both metrics.

Methods	ARI \uparrow (%)			NMI \uparrow (%)		
	Training	Validation	Test	Training	Validation	Test
ALADIN-ViT	79.2 \pm 3.0	76.2 \pm 3.9	77.5 \pm 3.5	93.9 \pm 0.7	96.0 \pm 0.6	96.5 \pm 0.5
CLIP	84.8 \pm 4.2	81.6 \pm 6.4	82.2 \pm 5.3	96.0 \pm 1.0	97.3 \pm 1.0	97.3 \pm 0.9
DINO	75.9 \pm 3.3	71.3 \pm 4.5	73.2 \pm 3.5	92.7 \pm 0.9	95.1 \pm 1.0	95.3 \pm 0.6
AbC CLIP	79.1 \pm 3.3	74.1 \pm 4.1	74.4 \pm 4.2	94.5 \pm 0.7	96.1 \pm 0.6	95.9 \pm 0.6
AbC DINO	85.1 \pm 2.6	83.2 \pm 3.8	84.7 \pm 3.7	96.0 \pm 0.7	97.4 \pm 0.7	97.7 \pm 0.6
CSD	84.1 \pm 3.0	82.2 \pm 3.4	82.0 \pm 3.7	96.0 \pm 0.7	97.4 \pm 0.6	97.5 \pm 0.6
Ours w/o cali	-	16.9 \pm 9.6	16.7 \pm 8.9	-	81.9 \pm 4.8	82.0 \pm 4.5
Ours	96.0\pm2.1	95.3\pm2.9	95.6\pm2.5	99.2\pm0.4	99.4\pm0.4	99.5\pm0.3

Table 3. The mean cosine similarity (\uparrow , $[-1, 1]$) between LoRA weight embedding and aggregated image feature embeddings derived from the same image set. ‘ALAD’ refers to ‘ALADIN-ViT’.

PC	ALAD	CLIP	DINO	AbC CLIP	AbC DINO	CSD	PC	ALAD	CLIP	DINO	AbC CLIP	AbC DINO	CSD
2	0.93	0.94	0.95	0.95	0.95	0.94	20	0.56	0.59	0.52	0.60	0.58	0.56
3	0.88	0.94	0.80	0.94	0.92	0.91	30	0.50	0.53	0.46	0.54	0.51	0.50
4	0.81	0.85	0.74	0.89	0.85	0.87	40	0.45	0.48	0.42	0.49	0.47	0.45
5	0.79	0.82	0.72	0.86	0.79	0.77	50	0.41	0.44	0.39	0.45	0.43	0.42
6	0.76	0.80	0.68	0.81	0.75	0.74	60	0.38	0.40	0.36	0.41	0.40	0.38
7	0.73	0.79	0.65	0.80	0.74	0.73	70	0.36	0.38	0.33	0.39	0.37	0.36
8	0.72	0.77	0.64	0.77	0.72	0.72	80	0.35	0.37	0.32	0.38	0.36	0.35
9	0.70	0.75	0.62	0.75	0.69	0.70	90	0.34	0.35	0.31	0.36	0.35	0.34
10	0.68	0.73	0.61	0.73	0.68	0.67	100	0.33	0.35	0.30	0.36	0.34	0.33

Table 4. Retrieval performance comparison between image-based features and our approach using full network weights across different scenarios. Higher is better for both metrics.

(a) Validation set performance.

Methods	mAP \uparrow (%)				Recall@24 \uparrow (%)			
	Orig+Orig	Orig+Gen	Gen+Orig	Gen+Gen	Orig+Orig	Orig+Gen	Gen+Orig	Gen+Gen
ALADIN-ViT	72.6	55.0	61.4	59.4	59.6	44.2	46.7	45.6
CLIP	83.3	73.9	76.3	73.4	70.1	60.6	61.7	58.9
DINO	70.5	66.5	63.6	63.6	53.4	49.8	46.9	47.0
AbC CLIP	81.3	72.0	73.6	70.9	66.8	59.0	58.2	56.5
AbC DINO	79.8	69.4	71.7	69.4	64.3	54.2	55.7	52.7
CSD	86.7	68.6	78.4	75.7	75.8	58.8	66.1	63.7
Ours w/o cali	32.3	32.3	32.3	32.3	20.4	20.4	20.4	20.4
Ours	83.9	83.9	83.9	83.9	71.4	71.4	71.4	71.4

(b) Test set performance.

Methods	mAP \uparrow (%)				Recall@24 \uparrow (%)			
	Orig+Orig	Orig+Gen	Gen+Orig	Gen+Gen	Orig+Orig	Orig+Gen	Gen+Orig	Gen+Gen
ALADIN-ViT	71.9	51.8	57.1	56.8	55.7	39.9	42.5	42.2
CLIP	80.0	69.7	71.3	70.5	66.2	56.6	58.6	56.2
DINO	67.2	61.4	61.7	60.5	51.6	48.0	45.9	45.3
AbC CLIP	78.1	69.8	70.5	68.4	65.0	56.9	56.3	54.1
AbC DINO	74.1	66.1	65.9	65.0	58.0	49.8	50.2	48.8
CSD	86.2	67.4	75.5	77.2	74.9	57.9	63.0	63.3
Ours w/o cali	31.4	31.4	31.4	31.4	19.5	19.5	19.5	19.5
Ours	83.4	83.4	83.4	83.4	69.4	69.4	69.4	69.4